Original Article

http://dx.doi.org/10.3348/kjr.2012.13.1.82
pISSN 1229-6929 · eISSN 2005-8330
Korean J Radiol 2012;13(1):82-89

Korean Journal of Radiology
KJR

Diffusion-Weighted Imaging of a Prostate Cancer Xenograft Model Seen on a 7 Tesla Animal MR Scanner: Comparison of ADC Values and Pathologic Findings

Dae Chul Jung, MD[1], Hak Jong Lee, MD[2], Jin Won Seo, MD[3], So Yeon Park, PhD[4], Sang Jin Lee, PhD[5], Joo Hyuk Lee, MD[6], In Hoo Kim, PhD[7]

[1]Department of Radiology, Yonsei University College of Medicine, Severance Hospital, Seoul 120-752, Korea; Departments of [2]Radiology and [4]Nuclear Medicine, Seoul National University College of Medicine, Seoul National University Bundang Hospital, Gyeonggi-do 463-707, Korea; [3]Department of Pathology, Hallym University Sacred Heart Hospital, Gyeonggi-do 431-070, Korea; [5]Genitourinary Cancer Branch, [6]Department of Radiology, and [7]Molecular Imaging & Therapy Branch, Research Institute and Hospital, National Cancer Center, Gyeonggi-do 410-769, Korea

Objective: To assess the relationship between apparent diffusion coefficient (ADC) values on diffusion-weighted magnetic resonance (MR) imaging and pathologic measures of a tumor using a prostate cancer xenograft model.

Materials and Methods: Eighteen athymic nude mice with 36 PC-3-induced tumors were sacrificed to obtain specimens immediately after MR imaging in order to compare the findings on MR images with those seen on pathological specimens. Using a high-field small-animal MR scanner, T1- and T2-weighted imaging and DW MR imaging was performed. Tumors were then processed for Hematoxylin and Eosin staining to evaluate tumor cellularity, intratumoral necrosis and immunostaining using antibodies directed against CD31 and vascular endothelial growth factor (VEGF) to determine the levels of microvessel density (MVD). Mean ADC values that were measured on the solid portion within each tumor were compared with tumor volume, cellularity, degree of necrosis, VEGF expression, and MVD in the corresponding section of the pathological specimen.

Results: Mean ADC values of the solid portion within the PC-3-induced high-grade tumors were significantly correlated with the degree of intratumoral necrosis ($r = 0.63$, $p < 0.0001$) and MVD ($r = -0.44$, $p = 0.008$) on pathologic slides. The ADC values were not significantly correlated with tumor cellularity, VEGF expression, or tumor volume in high-grade prostate cancer tissues.

Conclusion: In the xenografted prostate cancer model, the ADC values of the solid portion of the tumors are significantly correlated with tumor necrosis and MVD of the pathologic specimens. The ADC values may be utilized as surrogate markers for the noninvasive assessment of tumor necrosis and MVD in high-grade prostate cancer.

Index terms: *PC3; Prostate; Diffusion weighted imaging; MR; Necrosis; MVD*

Received June 30, 2011; accepted after revision August 18, 2011.
This work was supported from the Seoul National University Bundang Hospital Research Fund (grant no. 03-2008-002).

Corresponding author: Hak Jong Lee, MD, Department of Radiology, Seoul National University Bundang Hospital, 166 Gumi-ro, Bundang-gu, Seongnam-si, Gyeonggi-do 463-707, Korea.
• Tel: (8231) 787-7605 • Fax: (8231) 787-4011
• E-mail: hakjlee@radiol.snu.ac.kr

INTRODUCTION

Diffusion refers to the thermally driven random-walk motion of molecules. The distances travelled by diffusion of water molecules are strongly influenced by their local environment; therefore, it can be used for the probing of tissue microstructure on a scale comparable with cellular structures. Diffusion-weighted (DW) magnetic resonance (MR) imaging can be sensitive to microscopic displacements of water molecules using suitably arranged diffusion-weighting gradient pulses. Movement of water molecules in

Korean Journal of Radiology
KJR

tissue is not entirely random due to the inevitable presence of barriers to diffusion, such as the cell membrane and blood vessels. The apparent diffusion coefficient (ADC) provides a measure of the diffusion properties of the imaged tissue (1).

In recent years, there has been a significant growth in interest for the application of DW imaging to cancer. Both qualitative and quantitative DW MR imaging can be used in the evaluation of cancer *in vivo* for tumor characterization as well as for detection. Tumors differ in histological composition and this may reflect their biological aggressiveness. Both qualitative and quantitative DW imaging has been used for characterization of tumors in the brain, liver, kidneys, breast, uterus, and prostate (2-6). However, a considerable overlap in ADCs between study groups has been noted. It remains doubtful as to whether DW imaging can be used for the evaluation of microscopic structures of tumors with sufficient specificity to be useful in a clinical context. A major limitation of previous DW tumor imaging studies was the lack of correlation between pathological and imaging findings. Several previous reports have stated that such a correlation would likely require the use of animal models (7). Despite the increased use of DW imaging in oncology, no study examining the relationship between ADC and pathological variables using an animal model has been conducted.

The purpose of this study is to assess the relationship between ADC values on DW MR imaging and pathologic measures of tumors using a xenograft model of prostate cancer.

MATERIALS AND METHODS

The study was conducted with the approval of the Institutional Animal Care and Use Committee (IACUC) of the National Cancer Center (NCC) and the study conformed to the guidelines of the National Institutes of Health for the care and use of laboratory animals.

Tumor Model

Eighteen athymic male nude mice received subcutaneous injections of human cancer cells PC-3 on both flanks of the back in order to initiate tumors in each mouse (2 x 18 = 36 tumors). The PC-3 cancer cell line (American Type Culture Collection, Manassas, VA) was maintained as monolayers in E-MEM medium supplemented with 15% fetal bovine serum (FBS) at 37°C. Cells were harvested by trypsinization in trypsin/ethylenediaminetetraacetic acid (EDTA), washed in Hank's Balanced Salt Solution (HBSS) without Ca^{2+} and Mg^{2+}, and pelleted by centrifugation at 150 x g for 5 minutes. Subsequently, re-suspended cells were counted in a hemocytometer using 0.4% trypan blue, and brought to a final concentration of 1 x 10^6 cells/ml. Male, athymic nude mice (4-8 weeks old) were obtained from an animal facility (Orient, Seoul, Korea), housed under pathogen-free conditions, and maintained under controlled conditions (12-hour dark-light cycles; temperature, 20-24.8°C) with free access to sterilized mouse chow. Tumors were initiated by injection of approximately 1 x 10^6 cells per site (50 µl). Injections on each back flank were at least 20 mm apart and as far from the lung and heart as possible in order to minimize motion effects on MR imaging (Fig. 1).

Experimental Protocol

Initially, 36 tumors in 18 mice were imaged when the tumors reached 5-10 mm (shortest diameter), which was typically 2-4 weeks after implantation. In order to compare MR images and pathological specimens, 10 mice (20 tumors) were sacrificed for specimen preparation immediately after the initial MR imaging. The remaining eight mice (16 tumors) were sacrificed after the second MR imaging, eight days later. Next, tumors were excised and histologic analyses were performed.

MR Imaging and Histological Analysis

MR images were acquired using a high field (7.0 Tesla, 20 cm horizontal bore magnet) small-animal MR scanner (Bruker BioSpin, Rheinstetten, Germany). Animals were anesthetized with a continuous supply of 2% isoflurane (EZ Anesthesia, Palmer, PA) in air, placed in the prone position in the animal bed, and inserted into the radiofrequency coil (38 mm i.d.) inside the magnet. Scout transverse images were acquired for correct positioning of the pelvic region of the mouse. Different MR sequences were obtained in order to optimize tumor visualization and signal contrast. Fast T1-weighted (Bruker RARE sequence; field of view [FOV] = 3 x 2.5 cm, matrix = 256 x 256, spatial resolution = 117 x 98 µm/pixel, slice thickness = 1.0 mm, repetition time [TR] = 1300 ms, TEeff = 9.0 ms) and T2-weighted sequences (Bruker RARE sequence; FOV = 3 x 2.5 cm, matrix = 256 x 256, spatial resolution = 117 x 98 µm/pixel, slice thickness = 1.0 mm, TR = 2500 ms, TEeff = 36.0 ms) provided the best contrast, and were used for morphological examinations. The total acquisition time, including induction of

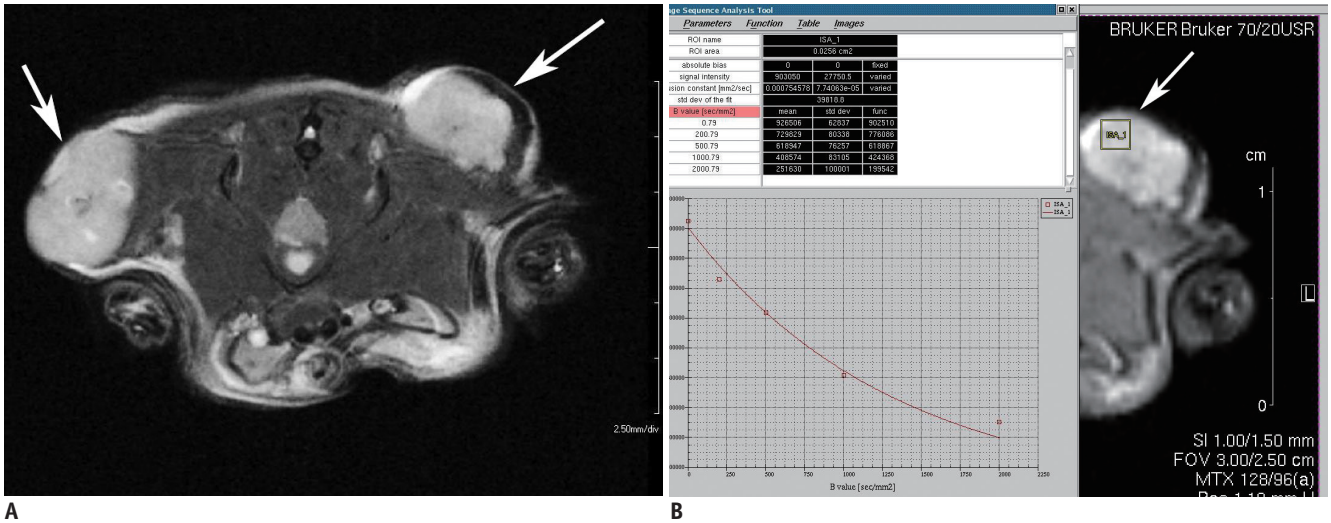

A B

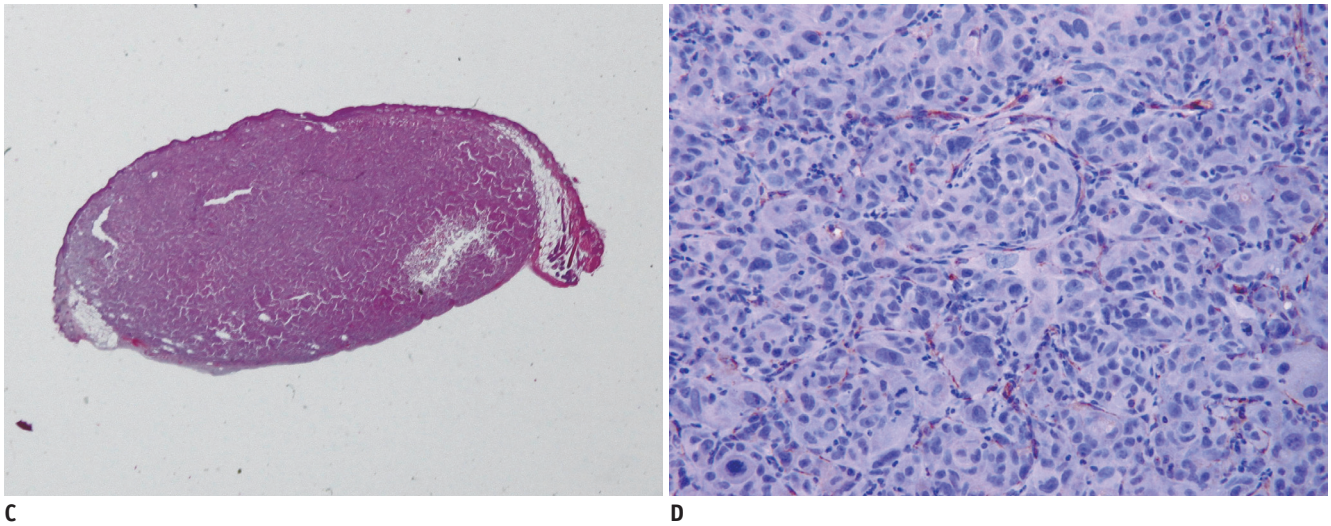

C D

Fig. 1. Human prostate cancer cell (PC-3) induced bilateral subcutaneous tumors on flank of athymic mouse.
A. T2-weighted MR images (Bruker RARE sequence; field of view = 3 x 2.5 cm, matrix = 256 x 256, spatial resolution = 117 x 98 μm/pixel, slice thickness = 1.0 mm, repetition time = 2500 ms, TEeff = 36.0 ms) of axial planes show homogeneous high signal intensity mass in injected area of both backs (arrows). **B.** Rectangular region of interest was placed within left tumor on axial plane of heavily T2 weighted MR image. Console program shows process of calculating apparent diffusion coefficient value of pixel area in region of interest. Apparent diffusion coefficient values for region of interest as well as apparent diffusion coefficient map could be calculated from following equation: Y = A + I * exp (-b * D). These parameters are defined as follows: Y: image intensity, A: absolute bias, I: multiplication constant, b: diffusion b-value and D: diffusion constant. This function (supplied by BRUKER®) uses b-value list calculated to generate x-axis. Fit is based on magnitude images of reconstructed data set using least squares mono exponential fitting. **C.** Photography of entire section (x 10) in pathological specimen stained with Hematoxylin and Eosin staining. Analysis program developed with visual C++ automatically performed calculation of percentage (%) of necrosis within tumor. **D.** Photomicrograph of immunohistochemical staining shows CD31 expression; microvessels stained with CD-31 were counted in four adjacent fields at x 200.

anesthesia, positioning, and set-up, was approximately 12 minutes per animal. After image acquisition, DW images were obtained using the Bruker SE-DWI protocol (FOV = 3 x 2.5 cm, matrix = 128 x 96, spatial resolution = 234 x 260 μm/pixel, slice thickness = 1.0 mm, TR = 2500 ms, TEeff = 26.0 ms, flip angle = 90°, excitations = 3). This protocol is based on the pulsed gradient spin echo (PGSE) sequence of Stejskal Tanner, with a series of four diffusion experiments/images. The diffusion gradient duration was 7 ms, while the diffusion separation time, D (big delta), was set to 14 ms. Three orthogonal gradient directions were applied in the DW MR. Corresponding b-values for the diffusion-sensitizing gradient were 0, 200, 500, 1000, and 2000 seconds/mm^2, respectively. ADC maps were constructed automatically on a pixel-by-pixel basis from the DW images for quantitative analysis. The ADC values were extracted from the experimental data from the indicated b-value ranging from 0 to 2000 s/mm^2 using a least squares

Korean Journal of Radiology
KJR

mono exponential fitting. During each imaging session, animal respiration rates and core-body temperatures were monitored continuously, with the temperature maintained via a feedback system that provided warm air to the bore of the magnet. Typically, the respiration rate was maintained at 40/min, and the core-body temperature was maintained between 35°C and 37°C.

The symbol '오' was used as an orientation marker in order to maintain proper orientation after tumor excision, where the upper round-shaped component 'ㅇ' of the symbol represents the cephalad direction, the mid vertical component 'ㅣ' of the symbol represents the mid vertical line of the tumor, and the lower horizontal line component 'ㅡ' represents the axial MR plane in the same orientation as the parallel line of the MR section at the most center level of the tumor. The orientation symbol was marked on skin overlying the tumor right after placement of the animal in the prone position in the animal bed inside the magnet. Although the skin marking is not visible on MRI, the horizontal line of the marking was considered closest to being parallel to the axial MR plane because the marking was made while holding the same MR position on the animal table inside the magnet. Animals were euthanized by CO_2 immediately after MR imaging. The gross findings were evaluated and recorded. Thereafter, we excised the tumor, including the overlying skin, where the orientation was marked. A total of 24 tumors were harvested within 24 hours after the last MRI. Histological slides were made at the NCC Histology Core Facility. The excised tissues were fixed in a large volume of 10% formalin for a minimum of one day to allow for complete tissue fixation. Histological examinations of all tissues were performed on paraffin-embedded sections. First, the paraffin block was bisected along the lower horizontal line component (ㅡ) on the overlying skin. Next, a serial section was made parallel to the sectional face. Subsequently, the block was sectioned along approximately the same plane as the axial MR images to permit the correlation calculation between the histological findings and MR images. Consecutive 5-μm sections were cut and mounted on glass slides. Sections were stained with Hematoxylin and Eosin (H&E). Expression of vascular endothelial growth factor (VEGF) was examined immunohistochemically with an anti-VEGF mouse monoclonal antibody (1:80, sc-7269; Santa Cruz Biotechnology, Fremont, CA) using the streptavidin-peroxidase technique with a SPTM kit (Zymed Laboratories, South San Francisco, CA). Polyclonal antibody (sc-1506r; Santa Cruz Biotechnology) against PECAM1 (CD31) was used for microvessel staining using the LSAB method (LSAB kit; Dako, Glostrup, Denmark). Negative controls were prepared by substitution of phosphate buffered saline for the primary antibody, and known positive controls were included for each staining procedure.

Tissue sections of the entire specimen were examined using a microscope at magnifications ranging from x 40 to x 400 by a board-certificated pathologist specially trained in genitourinary pathology. Features including tumor cellularity, angiogenesis, and degree of tumor necrosis, were analyzed for comparison with ADC values. For assessment of cellularity, four different areas of the slides (counterstained with H&E) were evaluated on x 400 high power fields (HPFs); in each case, the selection was made by a pathologist using an Olympus BX50 microscope (Olympus Co., Tokyo, Japan) and sections were photographed using a Spot Insight 2MP Firewire Color Mosaic Digital Microscope Camera (Diagnostic Instruments Inc., Sterling Heights, MI). Tumor cells included in each digital photograph were independently counted by two trained investigators and mean cellular number per one HPF was calculated in each case (8). The average score of the four areas was recorded. Microvessel density (MVD) was evaluated according to a previously described method (9). MVD within a designated hot spot (the most intensely neovascularized area at x 40 low power field) was scored on HPFs (x 200). Microvessels stained with CD-31 were counted on HPFs and the average score of the four areas was recorded. VEGF expression was semiquantitatively graded into four levels according to the percentage of positive tumor cells in the corresponding area. VEGF-positive tumor cells were not present in the examined tumor region for grade 0; VEGF-positive tumor cells were present in less than 25% for grade 1, between 25% and 50% for grade 2, and greater than 50% for grade 3 (10). For analysis of the degree of tumor necrosis, the pathologist marked necrotic areas on slides using a marking pen, according to a subjective decision of the pathologist. Thereafter, images of the tumors were photographed at a magnification of x 10 and imported into a Windows program that was developed with visual C++ using open source library CxImage, which performed calculation of percentage (%) of necrosis within the tumor (Fig. 1).

Data Analysis

Apparent diffusion coefficient values were computed and analyzed for each region, as compared with corresponding

regions on pathological specimens. A region-of-interest (ROI) that was minimally smaller than the actual solid portion of the lesion was carefully placed to ensure that cystic or necrotic areas were not included. Mean ADC values were then obtained after repeated measurement (3 times per tumor) (Fig. 1). Quantitative analysis of DW MR imaging, such as ADC measurement and drawing ROI, was performed by two experienced radiologists in consensus, who were unaware of the detailed pathologic findings. Three-dimensional volumetric measurements were used for assessment of tumor volume. In all contiguous axial images, tumor mass was outlined on the computer monitor using software (Rapidia 2.8, Infinitt, Seoul, Korea). The area of tumor in each slice was multiplied by the slice profile, and total tumor volume was automatically calculated by summation of the adjacent volumes.

Computed mean ADC values within solid portions of a mass on DW MR images were compared with pathological parameters, including tumor volume (measured on MR images), cellularity, MVD, VEGF expression, and tumor necrosis on corresponding sections of pathological specimens. Tumor necrosis on histological examination was defined as intratumoral necrosis that represents the fractional necrotic area in the entire section. For each tumor, the mean ADC value was plotted against the pathological parameters. The Pearson's correlation test was used for identification of correlation between pathological parameters and ADC values. A p value less than 0.05 was considered significant. All analyses were performed using Windows-based statistical software (STATA 10.0, Stata, College Station, TX; S-Plus 6.2, Insightful, Seattle, WA).

RESULTS

Tumors were seen as hyperintense on T2-weighted images, compared with adjacent intraperitoneal and subcutaneous tissues. On DW images, all xenografts were clearly shown as an increased area of intensity corresponding to the tumor on T2-weighted images (Fig. 1). The mean (± standard deviation [SD]) ADC value of PC-3-induced tumors was $0.86 \pm 0.17 \times 10^{-3}$ mm^2/sec, ranging from 0.64 to 1.14 ($\times 10^{-3}$ mm^2/sec). All PC-3 induced tumors were composed entirely of high-grade tumor, Gleason score 10 (5 + 5), pathologically.

Table 1 shows a summary of the correlation between DW MR parameters, including ADC values and pathologic findings for all tumors. ADC values of solid portions within PC-3-induced tumors showed significant correlation with the degree of intratumoral necrosis (correlation coefficient $r = 0.63$, $p < 0.0001$) and MVD ($r = -0.44$, $p = 0.008$) on corresponding pathologic slides. ADC values did not show significant correlation with tumor cellularity, VEGF expression, or tumor volume. The difference in ADC values between the initial and eight days after groups was not significant (Mann-Whitney U test, $p = 0.19$). Tumor cellularity ranged from 61 to 275 cells per HPF (median, 133 cells per HPF; SD, 58.3 cells per HPF) for the 36 PC-3-induced tumors. A linear relationship was observed between the ADC value and tumor necrosis or MVD on corresponding pathologic slides (Fig. 2).

DISCUSSION

Theoretically, more cellular tumors (tumors with more cells per unit volume) would be expected to show restricted diffusion (lower ADC values) compared with less cellular tumors. Some previous studies have shown lower water diffusibility in high-grade gliomas, as compared to lower grade gliomas (8, 11, 12). However, there is a considerable overlap between the ADC values for high-grade tumors and ADC values for low-grade tumors (7). It remains doubtful as to whether DW imaging can be used for evaluation of tumor grade with sufficient specificity to be useful in a clinical context. Some researchers have recently reported a significant inverse correlation between tumor cellularity and the ADC value in breast and prostate cancer patients

Table 1. Correlation Coefficient between ADC on DW MR Images and Pathologic Findings

Pathologic Findings	Mean ± SD	Correlation Coefficient to ADC
Necrosis (%)	15 ± 17.4	0.634 ($p < 0.0001$)*
MVD (No. per HPF)	11 ± 5.1	-0.436 ($p = 0.008$)*
Volume (mm^3)	37 ± 27.2	-0.054 ($p = 0.76$)
Cellularity (No. per HPF)	145 ± 58.4	-0.14 ($p = 0.41$)

Note.— *Indicates statistically significant value ($p < 0.05$). ADC = apparent diffusion coefficient, DW MR = diffusion-weighted magnetic resonance, HPF = high-power field, MVD = microvessel density, SD = standard deviation

Korean Journal of Radiology
KJR

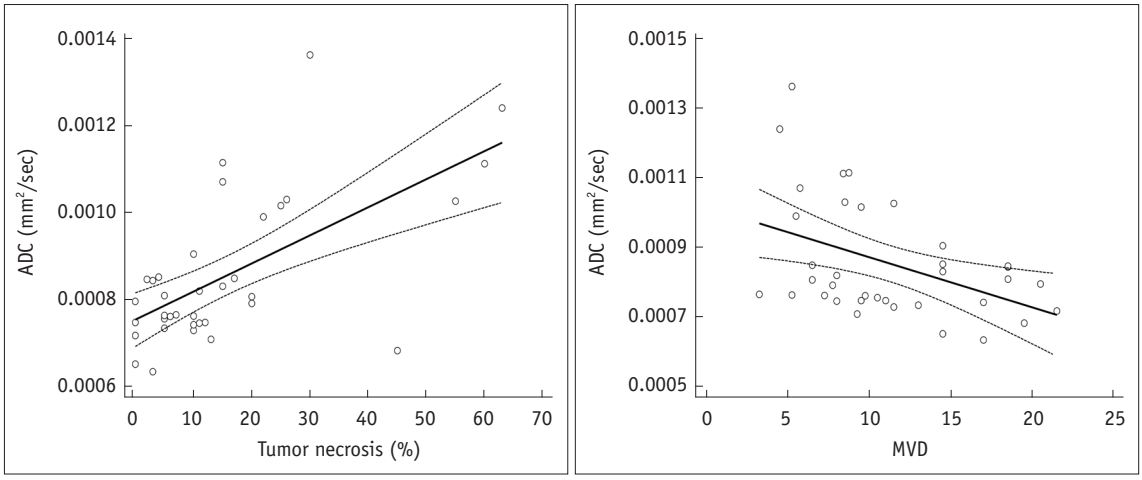

Fig. 2. Scatter plots of with regression line of apparent diffusion coefficient (ADC) value (mm^2/s) of high-grade prostate cancer xenograft.

A. Scatter plot with regression line between tumor necrosis (%) and mean apparent diffusion coefficient value. Linear relationship was found between mean apparent diffusion coefficient value and tumor necrosis ($R^2 = 0.402$, F-ratio = 22.89, $p < 0.001$). **B.** Scatter plot with regression line between microvessel density (MVD) and mean apparent diffusion coefficient value. There was linear relationship between mean apparent diffusion coefficient value and microvessel density ($R^2 = 0.19$, F-ratio = 7.96, $p = 0.008$).

(4, 5, 13-16). Others have shown the opposite result, with no relationship between them in patients with brain tumors (17). In the present study, PC-3 induced tumors that were composed entirely of high-grade tumors, above Gleason score 10 (5 + 5); therefore, pathologically, we did not know whether ADC values for high-grade tumors are different from those for low-grade tumors. However, our study using a xenograft model of prostate cancer has shown that the ADC values were not significantly associated with tumor cellularity within the range of the high-grade tumor. Other non-cancer cells and tissues such as glands, fibrous tissues, and stromal cells may contribute to restricted diffusion. In addition, the extracellular matrix may influence ADC more than cellularity within these high-grade ranges (17, 18).

The amount of signal loss in DW MRI is dependent on a number of factors. Diffusion in tissues is largely restricted by obstacles, mainly cell membranes. Water diffusion can also be restricted by a wall of microvasculatures as well as by the cell membranes between different cells. Because highly vascular tissues will differ from tissue with low vascularity in terms of water distribution, we expected that there would be a corresponding difference in ADC values between these two types of tissue (19). We initially hypothesized a relationship between the ADC value and tumor vascularity as represented by MVD. Angiogenesis plays a central role in survival of tumor cells for local tumor growth and for the development of distant metastasis. Although intratumoral neoangiogenesis is a very complex process, several investigators have suggested that the measurement of the MVD tumors might be of prognostic value. In particular, studies of prostate carcinomas have found MVD to be independently predictive of outcome (20-22). Our results also showed significant association between ADC values and MVD. The correlation was negative between them, which was consistent with our hypothesis. Although VEGF plays an important biological role in tumor angiogenesis, no significant association was observed between VEGF expression and the ADC value of the tumors in our study. Heo et al. (6) reported the same negative results in a study of patients with hepatocellular carcinoma. They indicated that the relationship between VEGF expression and the ADC value could not be explained by the role of VEGF as only a factor that increases capillary permeability (23). Selection bias and high-grade prostate cancer showed a low level of VEGF expression in most cases in the present study, which may be the reason that VEGF expression was not associated with the ADC value in our study.

Findings from our study have shown that only intratumoral necrosis was significantly associated with ADC values of solid portions within tumors. Tumor necrosis was characterized by increased membrane permeability and breakdown of the cell membrane, which resulted in free diffusion and an increase in the mean free-path length of diffusing molecules. These changes resulted in increased diffusion of water molecules in necrotic portions of tumors.

Recent animal experiments have also shown a remarkable correlation between ADC values and tumor necrosis (24, 25).

There are several limitations in the present study. We did not investigate DW MR imaging in a low-grade prostate cancer model or normal prostate tissue, which may provide additional information. However, xenograft models of prostate cancer cannot inherently represent the full spectrum of the disease. We believe that orthotopic implantation or use of a transgenic mouse model of prostate cancer may resolve these problems. Second, for the same technical reason, we cannot provide ADC values of normal prostate tissue. Contrary to our expectations, ADC values were not significantly changed in the delayed imaging group, as compared with the initial DW MR imaging. We believe that a larger number of subjects may have resulted in an improvement in the statistical power. Finally, we performed a monoexponential curve analysis; despite the multiple analytic approaches to DW MRI, such as bi-exponential curve analysis, some reports have shown that bi-exponential analysis was useful in some clinical settings, including prostate cancer, and it is not clear which is the best for a given situation, or what is the optimal set of b values that will influence the ADC values (2, 26-28). In the present study, the fit was performed using a least squares monoexponential fitting. A typical example is shown in Figure 1B. Monoexponential fitting using the total set of available b-values yielded the ADC (ADC_{mono}). Direct calculation of the ADC value using only 2-b values from the list of b-values was also performed. $ADC_{0\text{-}b}$ is the measured ADC, using the diffusion-weighted data from the b-value 0 and selected b values ranging from 200 to 2000 s/mm^2. Finally, only $ADC_{0\text{-}200}$ was different from ADC_{mono} ($p = 0.02$). Otherwise, for $ADC_{0\text{-}500}$, $ADC_{0\text{-}1000}$, and $ADC_{0\text{-}2000}$, there were no significant differences compared to ADC_{mono}; however, we can indicate that ADC was partially different than the methods of calculation (between monoexponential method and direct calculation using only 2 b-values). Due to these limitations, this study should be viewed as preliminary and, a larger scale study would be needed using various analytic methods including bi-exponential analyses to confirm our conclusions.

In conclusion, the ADC values of the solid portions within PC-3 induced high-grade tumors and did not reflect tumor cellularity and VEGF expression, while intratumoral necrosis and vascularity (MVD) showed a significant correlation with ADC values. DW MR imaging allowed visualization and quantification of intratumoral necrosis and MVD in a prostate xenograft model with correlation with ADC mapping to findings from the pathological specimens. ADC values may be utilized as a surrogate marker for the noninvasive assessment of intratumoral necrosis and MVD in high-grade prostate cancer.

Acknowledgments

The authors would like to thank Daehong Kim and Jae Gu Seong for small animal imaging. The authors would also like to thank You Chang Cho for digital image processing.

REFERENCES

1. Patterson DM, Padhani AR, Collins DJ. Technology insight: water diffusion MRI--a potential new biomarker of response to cancer therapy. *Nat Clin Pract Oncol* 2008;5:220-233
2. Padhani AR, Liu G, Koh DM, Chenevert TL, Thoeny HC, Takahara T, et al. Diffusion-weighted magnetic resonance imaging as a cancer biomarker: consensus and recommendations. *Neoplasia* 2009;11:102-125
3. Koh DM, Collins DJ. Diffusion-weighted MRI in the body: applications and challenges in oncology. *AJR Am J Roentgenol* 2007;188:1622-1635
4. Park MJ, Cha ES, Kang BJ, Ihn YK, Baik JH. The role of diffusion-weighted imaging and the apparent diffusion coefficient (ADC) values for breast tumors. *Korean J Radiol* 2007;8:390-396
5. Kim JK, Jang YJ, Cho G. Multidisciplinary functional MR imaging for prostate cancer. *Korean J Radiol* 2009;10:535-551
6. Heo SH, Jeong YY, Shin SS, Kim JW, Lim HS, Lee JH, et al. Apparent diffusion coefficient value of diffusion-weighted imaging for hepatocellular carcinoma: correlation with the histologic differentiation and the expression of vascular endothelial growth factor. *Korean J Radiol* 2010;11:295-303
7. Kono K, Inoue Y, Nakayama K, Shakudo M, Morino M, Ohata K, et al. The role of diffusion-weighted imaging in patients with brain tumors. *AJNR Am J Neuroradiol* 2001;22:1081-1088
8. Sugahara T, Korogi Y, Kochi M, Ikushima I, Shigematu Y, Hirai T, et al. Usefulness of diffusion-weighted MRI with echo-planar technique in the evaluation of cellularity in gliomas. *J Magn Reson Imaging* 1999;9:53-60
9. Gasparini G, Harris AL. Clinical importance of the determination of tumor angiogenesis in breast carcinoma: much more than a new prognostic tool. *J Clin Oncol* 1995;13:765-782
10. Yamaguchi R, Yano H, Iemura A, Ogasawara S, Haramaki M, Kojiro M. Expression of vascular endothelial growth factor in human hepatocellular carcinoma. *Hepatology* 1998;28:68-77
11. Bulakbasi N, Kocaoglu M, Ors F, Tayfun C, Ucoz T. Combination of single-voxel proton MR spectroscopy and apparent diffusion coefficient calculation in the evaluation of common brain tumors. *AJNR Am J Neuroradiol* 2003;24:225-233
12. Kim JH, Lim MK, Jeon TY, Rha JH, Eo H, Yoo SY, et

al. Diffusion and perfusion characteristics of MELAS (mitochondrial myopathy, encephalopathy, lactic acidosis, and stroke-like episode) in thirteen patients. *Korean J Radiol* 2011;12:15-24
13. Woodhams R, Kakita S, Hata H, Iwabuchi K, Umeoka S, Mountford CE, et al. Diffusion-weighted imaging of mucinous carcinoma of the breast: evaluation of apparent diffusion coefficient and signal intensity in correlation with histologic findings. *AJR Am J Roentgenol* 2009;193:260-266
14. Wang XZ, Wang B, Gao ZQ, Liu JG, Liu ZQ, Niu QL, et al. Diffusion-weighted imaging of prostate cancer: correlation between apparent diffusion coefficient values and tumor proliferation. *J Magn Reson Imaging* 2009;29:1360-1366
15. Zelhof B, Pickles M, Liney G, Gibbs P, Rodrigues G, Kraus S, et al. Correlation of diffusion-weighted magnetic resonance data with cellularity in prostate cancer. *BJU Int* 2009;103:883-888
16. Tan CH, Wang J, Kundra V. Diffusion weighted imaging in prostate cancer. *Eur Radiol* 2011;21:593-603
17. Jenkinson MD, du Plessis DG, Smith TS, Brodbelt AR, Joyce KA, Walker C. Cellularity and apparent diffusion coefficient in oligodendroglial tumours characterized by genotype. *J Neurooncol* 2010;96:385-392
18. Matsumoto Y, Kuroda M, Matsuya R, Kato H, Shibuya K, Oita M, et al. In vitro experimental study of the relationship between the apparent diffusion coefficient and changes in cellularity and cell morphology. *Oncol Rep* 2009;22:641-648
19. Jansen JF, Koutcher JA, Shukla-Dave A. Non-invasive imaging of angiogenesis in head and neck squamous cell carcinoma. *Angiogenesis* 2010;13:149-160
20. Weidner N, Carroll PR, Flax J, Blumenfeld W, Folkman J. Tumor angiogenesis correlates with metastasis in invasive prostate carcinoma. *Am J Pathol* 1993;143:401-409
21. Poon RT, Ng IO, Lau C, Yu WC, Yang ZF, Fan ST, et al. Tumor microvessel density as a predictor of recurrence after resection of hepatocellular carcinoma: a prospective study. *J Clin Oncol* 2002;20:1775-1785
22. Pruneri G, Ponzoni M, Ferreri AJ, Decarli N, Tresoldi M, Raggi F, et al. Microvessel density, a surrogate marker of angiogenesis, is significantly related to survival in multiple myeloma patients. *Br J Haematol* 2002;118:817-820
23. Sun HC, Tang ZY. Angiogenesis in hepatocellular carcinoma: the retrospectives and perspectives. *J Cancer Res Clin Oncol* 2004;130:307-319
24. Lang P, Wendland MF, Saeed M, Gindele A, Rosenau W, Mathur A, et al. Osteogenic sarcoma: noninvasive in vivo assessment of tumor necrosis with diffusion-weighted MR imaging. *Radiology* 1998;206:227-235
25. Vossen JA, Buijs M, Geschwind JF, Liapi E, Prieto Ventura V, Lee KH, et al. Diffusion-weighted and Gd-EOB-DTPA-contrast-enhanced magnetic resonance imaging for characterization of tumor necrosis in an animal model. *J Comput Assist Tomogr* 2009;33:626-630
26. Shinmoto H, Oshio K, Tanimoto A, Higuchi N, Okuda S, Kuribayashi S, et al. Biexponential apparent diffusion coefficients in prostate cancer. *Magn Reson Imaging* 2009;27:355-359
27. Mulkern RV, Barnes AS, Haker SJ, Hung YP, Rybicki FJ, Maier SE, et al. Biexponential characterization of prostate tissue water diffusion decay curves over an extended b-factor range. *Magn Reson Imaging* 2006;24:563-568
28. Klauss M, Lemke A, Grunberg K, Simon D, Re TJ, Wente MN, et al. Intravoxel incoherent motion MRI for the differentiation between mass forming chronic pancreatitis and pancreatic carcinoma. *Invest Radiol* 2011;46:57-63